SAN ONOFRE UNITS 2 AND 3

DOCKETS 50-361 and 50-362

CEN-165-(S)-NP

RESPONSES TO NRC CONCERNS ON APPLICABILITY OF THE CE-1 CORRELATION TO THE SONGS FUEL DESIGN

May, 1981

COMBUSTION ENGINEERING, INC.
NUCLEAR POWER SYSTEMS
POWER SYSTEMS GROUP
WINDSOR, CONNECTICUT 06095

LEGAL NOTICE

ABSTRACT

This document develops in detail, data which supports the position that CE-1 is applicable to the SONGS fuel design. This is accomplished with statistical analyses of critical heat flux (CHF) data, mechanistically based explanations of the CHF data obtained and supporting documents in the literature.

The following conclusions are made:

- The presence of the HID-? spacer grids has a beneficial effect on critical heat flux. Extrapolation of BWR experimental data to PWR conditions is invalid.

- When applied to non-uniform axial power distributions, the CE-1 correlation produces conservative results. The reasons for this conservatism are known.

- Reduction of the data base for CE-1 to include only the primary indication of DNB, results in essentially the same statistics for the correlation.

- Detailed statistical analysis of the data base for CE-1 demonstrates that there is no statistically significant difference attributed to the change from 14x14 to 16x16 fuel designs.

The document addresses all currently known NRC concerns. The results conclusively demonstrate the validity of the CE-1 correlation for a MDNBR of 1.13 but presents a still more conservative value of 1.19. They also show that there is no technical basis for further analytical or test efforts.

TABLE OF CONTENTS

I. SUMMARY

During the recent review of the SONGS 2/3 licensing submittals, a number of NRC staff questions have been raised relative to the applicability of the CE-1 critical heat flux (CHF) correlation to the high impact grid design of the SONGS 2/3 fuel assemblies.

The particular concern is the applicability of CE-1 to C-E's HID-2 grid design. The design characteristics of this grid are compared to other C-E grid designs in Table I-1.

This document provides responses to several concerns that have been expressed by the staff. The first concern is that the generally larger HID-2 grid causes a flow stagnation effect upstream of the grid to such an extent that the minimum departure from nucleate boiling ratio (MDNBR) is degraded. This is an effect which has been discussed in the literature under BWR conditions. Section II of this document addresses this concern and cites a number of references which support C-E's contention that the alleged effect is inconsequential. Based on this literature we conclude that it is not clear for the BWR conditions whether the effect of grids is beneficial or adverse. Furthermore, the conditions which might cause the effect to be adverse in BWR's do not occur for the HID-2 grid under PWR conditions. All experimental evidence from PWR tests shows grids to have a beneficial effect. This beneficial effect is believed to occur via the mechanisms discussed in Section III. This same mechanism provides the explanation of why C-E's non-uniform axial power distribution (APD) data has more scatter and is more conservative than the uniform APD data.

The second concern expressed by the staff was that "multiple data points have been used for some heater rods with quadrant instrumentation in non-matrix subchannels". This concern is addressed in Section IV which provides the results of a reanalysis of the data witnout use of the multiple data points. The results of this reanalysis show the revised statistics to compare very favorably with the original CE-1 data base statistics and continue to support an overall 95/95 MDNBR of 1.13. This is further evidence that the design MDNBR of 1.19 is adequately conservative to account for any uncertainties associated with the SONGS 2/3 high impact fuel design using HID-2 grids.

Another concern expressed by the staff is that C-E's non-uniform APD data from 14x14 and 16x16 designs "may not come from the same population". This concern is addressed in Section V. This section provides the details and the conclusions of an analysis of variance that was performed for both uniform and non-uniform APD data. This analysis shows statistically conclusive results supporting the fact that the variance between bundle types (i.e., 14x14 vs. 16x16) is very small, and therefore, the effect of the 14x14 vs. 16x16 design on the measured to predicted ratio is not statistically significant.

The attached sections address all of the concerns discussed to date and provide continued evidence that the CE-1 correlation is applicable to and in fact conservative for the SONGS 2/3 fuel design. It is also concluded that the method of application of the CE-1 correlation and the Tong F-factor as applied to SONGS 2/3 with a MDNBR of 1.19, provides substantial conservatism relative to the C-E committed DNBR criterion that the minimum DNBR shall provide at least a 95% probability with 95% confidence that DNB does not occur on a fuel rod having the MDNBR during steady state operation and anticipated transients of moderate frequency.

TABLE I-1

16 x 16 SPACER GRID CHARACTERISTICS

	ARKANSAS	SAN ONOFRE HID-1	SAN ONOFRE HID-2
GRID SPACING, INCHES	14.8	15.7	15.7
CLEAR SPACE BETWEEN GRIDS			
INTERIOR STRIP, INCHES			
PERIMETER STRIP, INCHES			
PERIMETER STRIP			
THICKNESS, INCHES			
HEIGHT, INCHES			
INTERIOR STRIP			
THICKNESS, INCHES			
HEIGHT, INCHES			

II. CRITICAL HEAT FLUX IN THE PRESENCE OF SPACER GRIDS

Introduction

Experiments have been performed to establish the effect of spacer grids on the Critical Heat Flux (CHF) in both BWR's and PWR's. At first glance, BWR test data appear to be inconclusive. Some data support the contention that spacer grids have a beneficial effect on CHF while other test data seem to show an adverse spacer grid effect. On the other hand, PWR test data consistently indicate that CHF is greater in the presence of spacer grids. The postulated mechanism associated with the BWR test data showing an adverse spacer grid effect will be examined in this section to determine whether such a mechanism could occur under PWR conditions.

One of the major thermal-hydraulic (T-H) differences between BWR's and PWR's is the typical flow regime that is present in the region of boiling crisis for the reactor. Subcooled and bubbly flow are usually encountered in PWR's while annular flow is predominant in BWR's (1).* The two types of flow regimes differ substantially, as shown in Fig. II-1.

Subcooled and bubbly flow regimes in PWR's are typically characterized by a relatively thin bubble layer on the fuel rods and a liquid core. On the other hand, annular flow is characterized by a thin liquid film and a vapor core. In BWR's, the liquid film associated with annular flow coats the fuel rods while the remaining subchannel area is filled with vapor.

Spacer grids are used in both BWR's and PWR's to maintain subchannel geometry. These grids disrupt the local flow in subchannels and thereby influence the T-H performance of the core. Since the flow regimes differ in BWR's and PWR's, and spacer grids affect T-H performance by disrupting subchannel flow, it is likely that the T-H effects of spacer grids will be different for BWR's and PWR's.

Results from several BWR and PWR tests will be discussed and conclusions will be made regarding the effects of spacer grids in PWR's. The postulated mechanism associated with adverse grid effects in BWR's will be examined to determine whether such a mechanism could exist in PWR's. While spacer grids disrupt local flow and thereby give rise to hydrodynamic and heat transfer effects, attention will be focused on the impact of these effects on CHF in the following discussion.

Effects of Spacer Grids in BWR's

Tests with 9 and 16 rod BWR test sections have shown that boiling crisis occurs preferentially upstream of spacer grids (2)(3). These test data indicate that spacer grids may either promote or delay boiling crisis, thereby decreasing or raising CHF, dependent on the coolant quality and the axial location of the grids. The authors concluded that CHF is affected by the flow redistribution caused by the presence of spacer grids, but determined that local disruption of the liquid film by the spacer grid

*Parenthetical numbers refer to similarly numbered documents in the REFERENCE section.

did not contribute to boiling crisis.

Adiabatic air/water tests were conducted at low pressures to determine the hydrodynamic effect of various flow obstructions (2) (4) (13). These tests simulate the flow conditions that occur in the annular flow regime, where a thin liquid film blankets the fuel pin and the remainder of the subchannel flow area is filled with vapor. Dry patches formed in front of the flow obstructions below critical air/water flow rates. These patches grew as the film flow rate was reduced. Dry patches also were observed just downstream of the obstructions.

Lahey and Moody have proposed that the upstream dry patches are caused by horseshoe vortices which form upstream of the flow obstruction, as shown in Fig. II-2.The vortices improve local mass transfer just upstream of the grid to the point where all the liquid is transferred from the surface to the free stream air flow. This results in the formation of a dry patch just upstream of the grid.

The mechanism for boiling crisis in annular flow is dryout of the liquid film (6). Hence, the hydrodynamic dryout which occurred in the adiabatic air/water tests is postulated to be the mechanism by which boiling crisis occurs upstream of BWR spacer grids.

Thus, BWR test data indicate that spacer grids may have either beneficial or adverse effects on boiling crisis. The postulated mechanism associated with the adverse effect of spacer grids is the formation of a horseshoe vortex upstream of the grid. It is important to note that this postulated mechanism best explains test data from idealized adiabatic air/water tests and may therefore have only limited applicability to actual diabatic BWR conditions.

Effects of Spacer Grids in PWR's

Many researchers have reported that the presence of spacer grids in PWR test sections has a beneficial effect on CHF because the grids deplete the bubble layer near the fuel and enhance turbulence and mixing. These three effects, depletion of the bubble layer, enhanced turbulence, and enhanced mixing will be referred to collectively as enhanced heat transfer.

Chang and Dean (7) noted the beneficial effect of spacer grids in their discussion of the effects of flow blockages on core power limits. Tong (8) has included a beneficial spacer factor in a CHF correlation to account for the beneficial effects of enhanced heat transfer on CHF. Other researchers (9) (10) have found that the heat transfer coefficient is increased in the presence of spacer grids.

An extensive survey by Groeneveld and Yousef (11) of experiments on the effects of spacer grids concluded that there is no deleterious upstream effect associated with spacer grids. Tests have, however, shown that boiling crisis occurs preferentially just upstream of PWR spacer grids. Groenveld and Yousef conclude that this preferential occurrence of boiling crisis is a result of the enhanced heat transfer that occurs downstream of the spacer grid, since

at the upstream edge of a spacer grid, the enhanced heat transfer associated with the previous spacer grid is at a minimum.

C-E has conducted uniform axial power distribution CHF tests with a spacer grid near the end of the heated length (12). These tests have shown that the presence of a spacer grid just downstream of the location of CHF has a negligible impact on the magnitude of CHF.

Hence, a considerable body of evidence indicates that PWR spacer grids:

1) have a beneficial effect on CHF downstream of the grid
2) have a negligible effect on CHF upstream of the grid

The CHF benefit associated with the presence of spacer grids is the result of enhanced heat transfer as the coolant passes through the grids. As explained earlier, subcooled and bubbly flow regimes are typically encountered near the boiling crisis in PWR's. A layer of bubbles clings to the fuel rods in this flow regime while the remainder of the subchannel is filled with subcooled liquid, as shown in Fig. II-1. A sketch of the projected area of a spacer grid in a matrix subchannel is shown in Fig. II-3. The flow obstruction presented by the intersection of grid strips in the center of the subchannel diverts "cold" water from the subcooled core of fluid in the subchannel toward the fuel rods. It is noteworthy that the flow obstruction presented in a typical subchannel by C-E spacer grids differs greatly from the obstructions used in the adiabatic air/water tests discussed earlier. The obstruction presented by the C-E grid lies primarily in the center of the subchannel while the obstructions used in the air/water tests and shown in Fig. II-2 were in contact with the channel wall over a large area.

The flow diversion associated with C-E grids has beneficial effects on heat transfer and CHF performance for several reasons. The diverted coolant must travel at a higher velocity to preserve continuity. The combination of higher velocity and cooler liquid near the fuel rod will strip the bubble layer from the fuel rod. Furthermore, heat transfer will be enhanced by the mere presence of cooler liquid near the fuel rod. Redistribution of coolant through the grid also increases the turbulence of the coolant, thereby increasing mixing and improving heat transfer.

The mechanism for boiling crisis in PWR's is departure from nucleate boiling (DNB). Boiling crisis occurs when bubbles generated at the fuel surface cannot escape from the surface faster than they are generated. This results in the formation of an insulating blanket over the surface of the fuel rod. The stripping away of bubbles by flow diverted by the spacer grids thus will postpone the onset of DNB.

Inapplicability of Adverse BWR Conclusions to PWR Conditions

It is unclear whether presence of spacer grids in BWR test sections has an adverse or beneficial effect on boiling crisis. PWR test data indicate that spacer grids have a beneficial effect on boiling crisis. The postulated mechanism associated with the adverse effect of spacer grids in BWR's is the formation of a horseshoe vortex just upstream of the spacer grid and the corresponding dryout of the liquid film at the "fuel" surface. This

mechanism will now be examined to determine whether such an effect is possible in C-E PWR's.

Formation of a horseshoe vortex in adiabatic air/water tests (6) improved mass transfer between the water film and air to the extent that dryout of the water film occurred. It is unlikely that such a vortex will form upstream of the obstruction presented by C-E spacer grids, since the grid obstruction differs greatly from the type of obstructions used in the air water tests. A comparison of Figs. II-2 and II-3 shows that the air/water test obstructions were in contact with the "fuel" surface over a large area while the obstruction presented by the spacer grid is located primarily in the center of the flow channel with relatively little fuel surface contact.

While the difference in geometry makes the formation of a vortex at the leading edge of the grid unlikely, such a vortex would have a beneficial effect on CHF at typical PWR conditions. A vortex upstream of a PWR spacer grid would improve heat transfer between the fuel surface and bulk coolant flow in a manner analogous to that in which mass transfer was improved in the air/water tests and also by bringing colder water closer to the fuel rod surface. This improved heat transfer would retard the formation of a vapor blanket at the fuel surface thereby increasing CHF. Hence, if a vortex did form upstream of a PWR spacer grid, it would have a beneficial effect on CHF.

Formation of vortices upstream of spacer grids is postulated to have an adverse effect on CHF in BWR's. It is unlikely that such vortices could form in PWR's because the obstruction created by the spacer grids in subchannels differ greatly from the types of obstructions considered in the air/water tests. However, if such vortices did form, local heat transfer would be improved and CHF would thus increase in PWR's. Therefore, none of the BWR test data can be used to demonstrate that spacer grids will decrease CHF in PWR's.

Conclusions

The flow regimes and mechanisms associated with boiling crisis are different in BWR's and PWR's. BWR's typically exhibit annular flow; dryout of the liquid film on the fuel rods is the mechanism for boiling crisis in this flow regime. Subcooled and bubbly flow are encountered in PWR's and DNB or vapor blanketing of the fuel is the mechanism for boiling crisis in PWR's.

BWR test data show both beneficial and adverse effects of spacer grids on CHF. The postulated mechanism for the adverse effect is the formation of a vortex upstream of the grid which accelerates dryout of the liquid film on the fuel. Because of the difference between the type of obstructions used in the tests that support the formation of vortices and the obstruction presented by C-E spacer grids in flow subchannels, it is unlikely that the vortices will appear in the flow subchannels. Even if vortices did form, they would improve heat transfer between the fuel surface and bulk coolant thereby increasing CHF in PWR's.

All PWR and some BWR test data demonstrate that CHF increases in the presence of spacer grids. It is unlikely that the postulated mechanism (vortex) associated with the adverse effect of spacer grids in BWR's can exist upstream of PWR grids. If this mechanism did exist in PWR's, it would be expected to increase CHF because the PWR flow regime differs from the BWR flow regime. Therefore, all experimental evidence indicates that spacer grids increase CHF in PWR's.

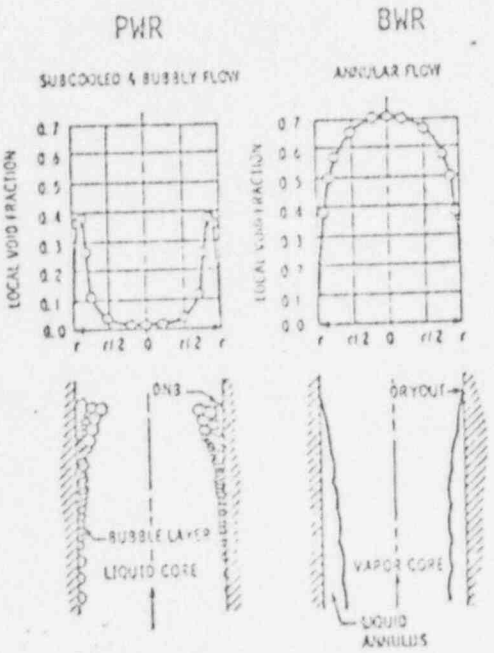

Figure II-1: Comparison of Flow Regimes Near Boiling Crisis in PWR's and BWR's (from Reference 1)

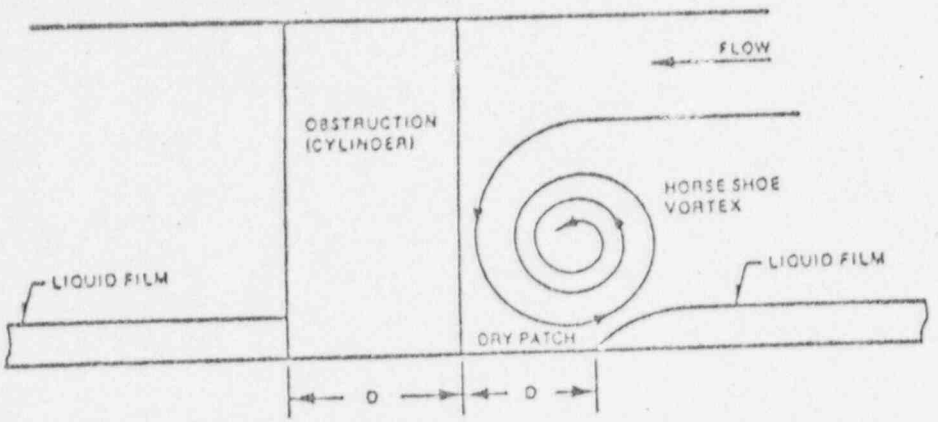

Figure II-2: Effect of Flow Obstruction on Liquid Film in Annular Flow (from Reference 5)

Figure II-3:Projected Area of C-E Spacer Grids in a Matrix Subchannel

III. EFFECTS OF SPACER GRIDS IN NON-UNIFORM APD CHF TESTS

Introduction

Spacer grids enhance heat transfer and have a beneficial effect on CHF in PWR rod bundles, as explained in Reference 8. Hence, observed CHF in PWR test sections is greater in the presence of spacer grids. The following discussion will demonstrate that the effect of spacer grids is amplified in non-uniform axial power distribution (APD) test sections. Enhanced heat transfer downstream of a grid postpones the occurrence of DNB until just upstream of the following grid. Thus, two effects are combined in non-uniform CHF tests. First CHF is greater because of the presence of the spacer grids; second, because CHF is delayed until just upstream of a spacer grid, the local heat flux is typically lower than would have been found in the absence of the grid.

The CE-1 correlation is based on uniform APD test data from test sections with standard C-E spacer grids. The correlation therefore implicitly contains the beneficial effect of these spacer grids in increasing CHF in uniform APD bundles. Tests have shown that boiling crisis occurs at lower local heat fluxes with non-uniform APD test sections than with their uniform APD counterparts. However, the CE-1 correlation does not include models to explicitly account for the effects of non-uniform APD's or the local effects of spacer grids within the grid span. The Tong F-factor is used with the CE-1 correlation to account for the effects of non-uniform APD's. However, the coefficients involved in the F-factor have not been re-optimized for use with the CE-1 correlation; nor have the correlation coefficients been re-optimized to accommodate the F-factor.

The use of the F-factor with the CE-1 correlation, with no explicit modeling of local grid effects in the correlation gives rise to conservatism and increased scatter in the data. The conservatism and increased scatter arise because of the real effects of spacer grids in the non-uniform test sections. The relationships between the effects of spacer grids and the increased conservatism and scatter will be explained qualitatively. This explanation demonstrates that the use of the CE-1 correlation in conjunction with the Tong F-factor yields conservative CHF predictions and is therefore suited for use in design analyses.

Description of Phenomenon

The CE-1 correlation (15) is based upon 731 data points from uniform APD sections with standard spacer grids. The distance between the uppermost spacer grid and the end of the heated length in these test sections was purposely made equal to the nominal grid spacing in order to provide the most conservative DNB test results. This design ensured that DNB occurred at the end of the heated length. Thermocouples in these test sections were located -0.5" below the end of the heated length. Depending on the test section under consideration, the thermocouples were located between [ ] downstream of the downstream edge of the uppermost spacer grid in the test sections. Spacer grids enhance heat transfer downstream of the grid; however, this enhancement decays with distance downstream of the grid. Hence, although the CE-1 data include a benefit resulting from the enhanced heat transfer downstream of the grid, the benefit is small, since the thermocouples are relatively far downstream of the spacer grids.

The effect of enhanced heat transfer on CHF for uniform APD's is illustrated in Fig. III-1, which shows a plot of CHF and local heat flux vs. distance from the test section inlet. Fig. III-1a shows the hypothetical CHF profile for a bare test section with no spacer grids. The CHF in this hypothetical test section starts out at its maximum value and decreases with distance from the inlet as quality increases. The power level is chosen such that DNB is observed at the end of the heated length for an average heat flux P_1.

The CHF profile for a uniform APD test section with grids is presented in Fig. III-1b. The CHF profile without grids is superimposed on Figure III-1b for reference. The effect of the spacer grids on CHF gives rise to the "sawteeth" in Figure III-1b. Immediately downstream of the spacer grid, the enhanced heat transfer increases the local CHF. Since the enhanced heat transfer decays with distance from the spacer grid, local CHF decreases with distance from the spacer grid. However, the effects of the enhanced heat transfer do not disappear completely before reaching the downstream grid. The enhanced heat transfer benefit associated with the grids gives rise to a higher CHF value at the end of the heated length. The test section with no spacer grids experienced CHF at the end of the heated length with an average heat flux P_1. The enhanced heat transfer associated with the presence of spacer grids causes the test section with grids to reach an average heat flux P_2 before experiencing DNB at the end of the heated length. The fact the P_2 is greater than P_1 is a direct result of the enhanced heat transfer associated with the spacer grid.

In summary, the presence of spacer grids in the test section has the following two effects on the observed CHF in uniform APD tests:

1) increase in CHF in crossing a spacer grid ("sawtooth effect")
2) increase in power (P_2 vs P_1) to DNB resulting from enhanced heat transfer at the end of the heated length.

The effects of grids in non-uniform APD test sections are more complicated than in uniform APD test sections because the location of DNB shifts in the non-uniform tests as a result of the spacer grid heat transfer enhancement. CHF profiles for two non-uniform APD test sections are presented in Fig. III-2. The CHF profile for a bare non-uniform test section without spacer grids is shown in Fig. III-2a.

A CHF profile for a non-uniform APD test section with spacer grids is shown in Fig.III-2b. The bare test section CHF profile is superimposed on Fig. III-2b for reference. As in the discussion of uniform APD test sections, the local "sawtooth" effect and the increased power level to DNB resulting from enhanced heat transfer in the presence of grids are apparent in Figure III-2b. A third effect also appears in the non-uniform APD test with grids.

DNB occurs at the intersection of the local heat flux profile and the CHF profile in Figs.III-2a and III-2b. The curves intersect at point A for the bare test section and point B for the test section with grids. A comparison of the CHF curves for the bare test section and the test section with grids in Fig. III-2b shows that both the power level at DNB and the location of DNB change because the grids are present. If the location of DNB did not change, the average heat flux could be increased to P_1'before the local heat flux and CHF profiles intersected at point A'. However, as power is increased above P_1, the local heat flux and CHF profiles intersect at point B at an average heat flux P_2. Thus, the location of DNB shifts due to the presence of grids. Three effects occur as a result of the presence of grids in non-uniform APD test sections:

1) local CHF increases in crossing a spacer grid ("sawtooth effect")
2) average power to DNB increases as a result of the enhanced heat transfer associated with spacer grids
3) location of DNB shifts to just upstream of a spacer grid because of the enhanced heat transfer associated with spacer grids.

Effect of Phenomenon on CHF Correlation

The CE-1 CHF correlation is based upon uniform APD test data from test sections with standard spacer grids. Part of the increase in power to DNB associated with the presence of spacer grids is therefore implicitly included in the CE-1 correlation, as explained earlier.

Measured and predicted CHF values for the CE-1 correlation with the Tong F-factor were compared for 4 test sections with nonuniform APD's in Reference 16. An evaluation of the measured to predicted (M/P) ratios showed that the predicted CHF was consistently lower than the measured value and that there was more scatter than for the uniform data (i.e., the standard deviation was larger). Both of these observations can be explained by the effects that arise from the presence of grids in non-uniform APD test sections.

As explained earlier, the presence of spacer grids increases the power to DNB and changes the location of DNB in non-uniform test sections. The consistent underprediction of CHF by the CE-1 correlation (with the Tong F-factor) is explained by the additional increase in CHF associated with the presence of spacer grids not accounted for by CE-1 and furthermore by the fact that the coefficients in the Tong F-factor were not recorrelated for use with CE-1.

The increased scatter in data for the non-uniform test data is also explained by the effect of the spacer grids. As already explained, the CE-1 correlation does not explicitly model the local effects (i.e., the "sawtooth effect") of spacer grids on CHF. Consequently, the correlation may not accurately predict the axial location of CHF in non-uniform test sections. Application of the CE-1 correlation in design analyses recognizes this and thus, Minimum DNBR is used as the design criterion regardless of the location. The location of DNB may be predicted at any axial level by the CE-1 correlation in the non-uniform test sections. However, the presence of spacer grids in the test sections causes DNB to occur just upstream of spacer grids. Consequently, when M/P ratios are computed for a particular test point, the predicted location of DNB generally differs from the observed occurrence of DNB. This difference in axial location results in the increased scatter found in the M/P data for non-uniform test sections.

The effect of the difference in predicted and actual location of DNB is shown in Fig.III-3. The CE-1 prediction line is shown tangent to a non-uniform heat flux profile labeled $q"_2$ (z) at the predicted DNB point. However, the actual CHF line, with spacer grid effects included, is above the prediction line except at locations immediately upstream of the spacer grids. Another non-uniform heat flux profile labeled $q_1"$ (z) is shown intersecting the actual CHF line at grid #2, the actual DNB location. The distance "X" between the two heat flux profiles represents the magnitude of CHF power underprediction that results from not including the spacer grid effect explicitly in the CE-1 correlation. The example shown in Fig. III-3 represents a case where the predicted DNB location

is approximately midway between two spacer grids. If the predicted location were at a spacer grid, the underprediction would be zero. Because the predicted locations will be more or less randomly distributed with respect to the spacer grids, the set of underpredictions, X_i, will have a mean greater than 1.0, and a variance. It is estimated that this mean and variance are of adequate magnitude to explain part of the conservatism of CE-1 when it is applied to the non-uniform data as well as most of the increased scatter. The remainder of the conservatism is due to the F-factor.

Thus the underprediction of CHF by the CE-1 correlation in non-uniform test sections results from the presence of spacer grids in the non-uniform test section and the fact that the coefficients of the Tong F-factor were not re-optimized for use with the CE-1 correaltion. The increased scatter in M/P ratios for non-uniform test data results from the fact that the CE-1 correlation includes no grid effects model and, consequently, the axial location of predicted and observed DNB differ because of the presence of spacer grids in the test section. Increased scatter also results from the use of a non-optimized F-factor which increases variance, as shown in Section V.

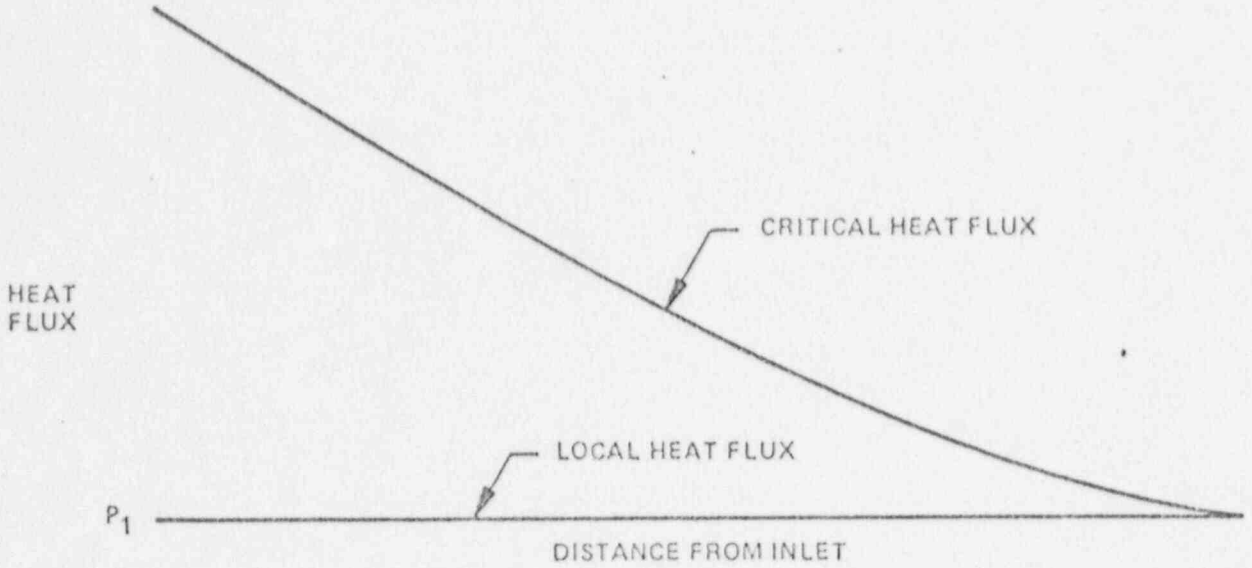

Figure III-1a
CHF PROFILE WITH UNIFORM APD AND NO GRIDS

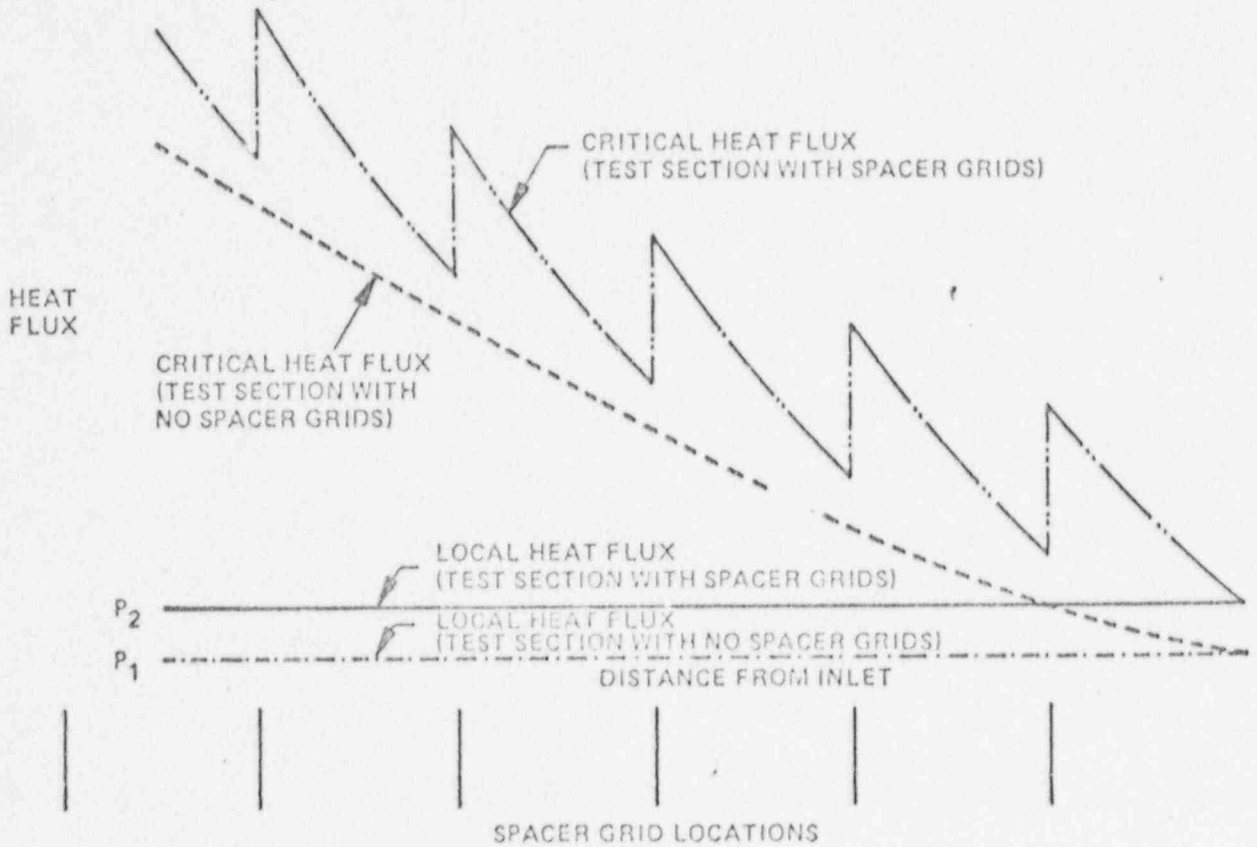

Figure III-1b
CHF PROFILE WITH UNIFORM APD AND SPACER GRIDS

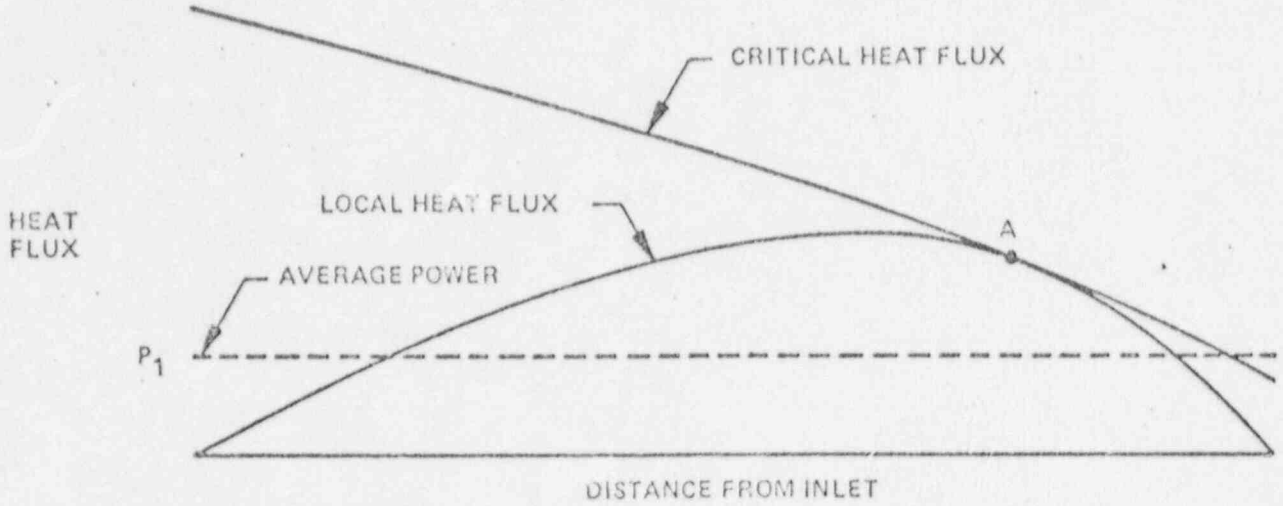

Figure III-2a
CHF PROFILE WITH NON-UNIFORM APD AND NO GRIDS

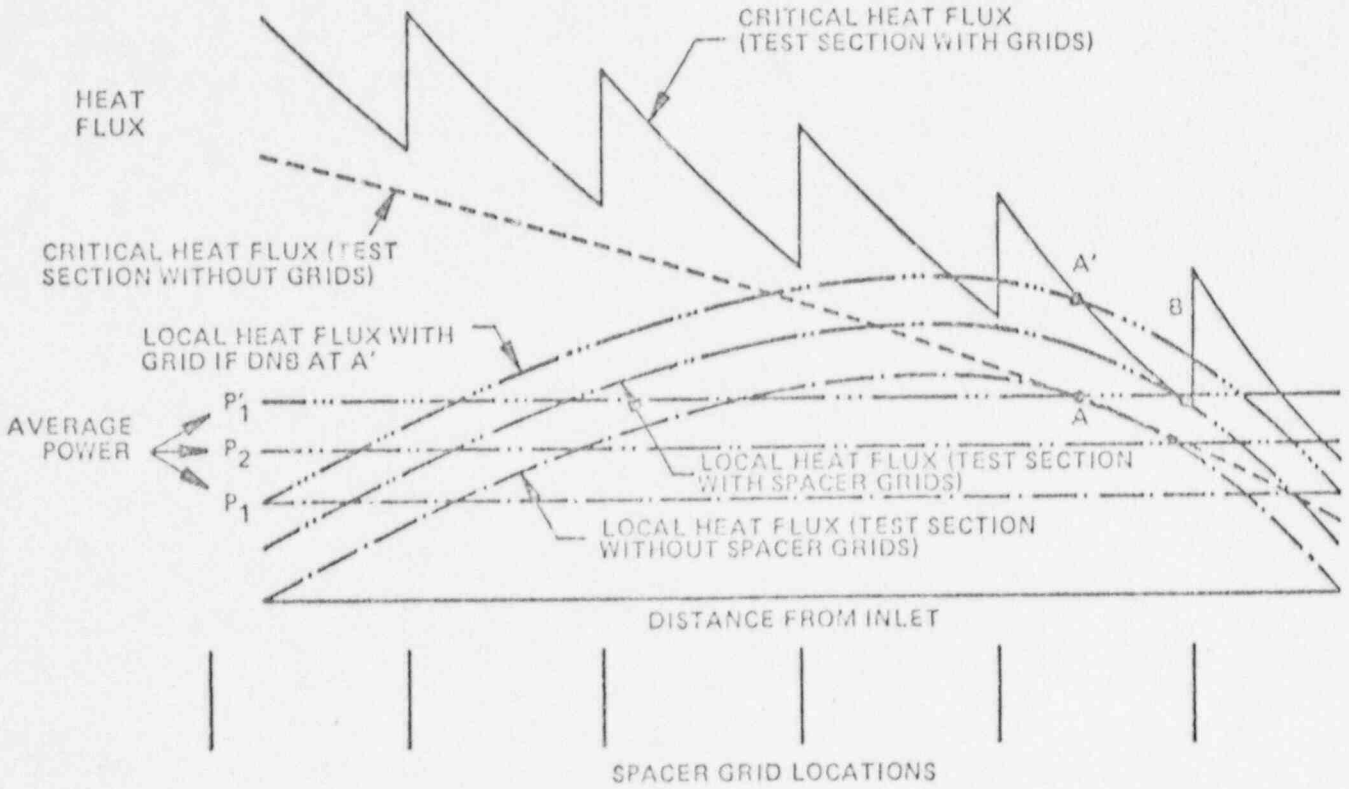

Figure III-2b
CHF PROFILE WITH NON-UNIFORM APD AND SPACER GRIDS

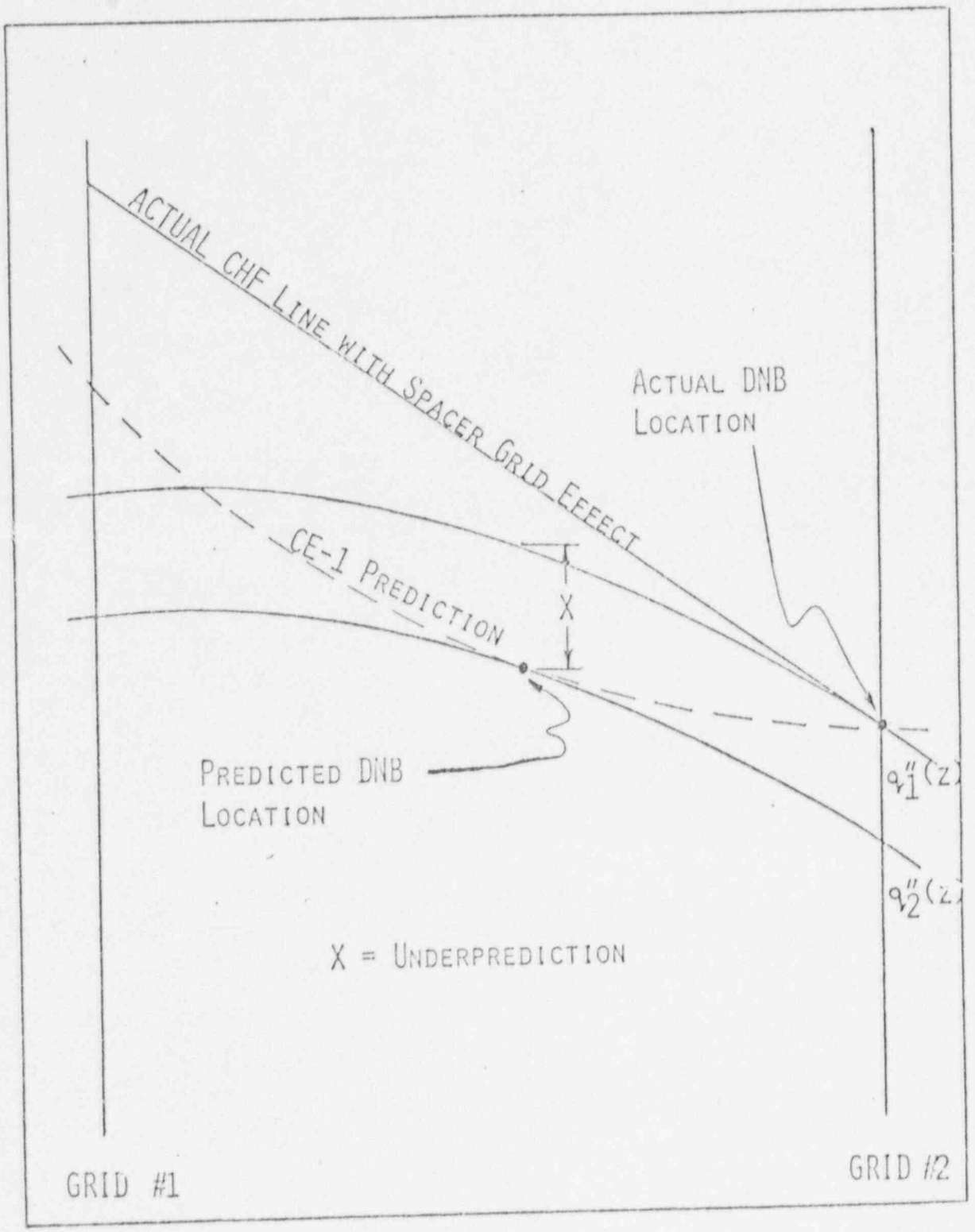

Figure III- 3:Effect of Difference Between Predicted and Actual Locations of DNB

IV. EFFECT OF MULTIPLE DATA POINTS

A stated concern of the NRC staff has been the use of multiple data points from the CHF tests. Multiple data points are those CHF indications during a test that arise because of the multiplicity of instrumented rods and thermocouples within a rod. The thermocouple which gives the very first indication of CHF during a test provides the data point identified as the primary indication. In most tests CHF indications occur at other thermocouple locations slightly later. These are identified as secondary indications. The use of primary and secondary indications in the development of CE-1 has prompted the following question on another docket. "In the development of the CE-1 correlation with uniform axial power distribution (CENPD-162), multiple data points have been used for some heater rods with quadrant instrumentation in non-matrix subchannels. Therefore, the statistical analysis should be re-performed by eliminating the redundant data points. Provide, based on the reduced data, new minimum DNBR limits for 14x14 and 16x16 rod bundles, separately and jointly".

A technically consistent response to this question would require re-correlation of the new subset of test data (i.e., the subset with "redundant" data points eliminated) to produce revised values for the constants in CE-1. In lieu of this, a conservative approximation to the requested information has been obtained by performing a statistical analysis of primary CHF indications only, using unrevised CE-1. This approach is conservative because the constants in CE-1, not being optimized for the data subset being examined, will introduce additional scatter into the resulting measured/predicted CHF ratios.

In Table IV-1 means and standard deviations for the ratio of measured/predicted CHF are shown using data for only the primary CHF indication in each test run. The corresponding 95/95 MDNBR limit is given separately for 14x14 and for 16x16 fuel types, as well as for the complete primary indication data set. For comparison, the same information is provided for the total CE-1 data base (including multiple indications).

It can be seen that the primary-indication-only statistics compare well with the total CE-1 data base statistics, and continue to support an overall 95/95 MDNBR limit of 1.13. This is further evidence that the design MDNBR limit of 1.19 is adequately conservative to account for any uncertainties associated with the SONGS high impact fuel design using HID-2 grids.

TABLE IV-1

COMPARISON OF TOTAL CE-1 DATA BASE
WITH PRIMARY DNB INDICATION SUBSET

Type		14x14			16x16			
No. Rods Length in ft.		21 7	21 12.5	25 7	21 7	21 12.5	25 7	TOTAL
n Number of Data Points	All Data	141	99	51	169	157	114	731
	Primary Data	72	45	37	70	52	55	331
μ Mean of $\frac{\text{CHF Meas.}}{\text{CHF Pred.}}$		[redacted]						
σ Standard Deviation of $\frac{\text{CHF Meas.}}{\text{CHF Pred.}}$								
95/95 MDNBR	All Data	1.132			1.139			1.133
	Primary Data	1.136			1.122			1.123

V. STATISTICAL EVALUATION OF CHF DATA

Introduction

In response to NRC requests, a statistical analysis has been performed on critical heat flux (CHF) data from C-E CHF experiments. The data evaluated are those from experiments with both uniform and non-uniform axial power distributions (APD). The analysis was performed to determine if there is a statistically significant effect of bundle type (i.e., 14x14 vs. 16x16) and to establish the significance of test section length for the uniform data using the methodology of Reference 17.

To perform this calculation, analysis of variance is used. This approach allows one to extract from the total variance for the experiments, the components of variance between groups (e.g. bundle type), between test sections and within test sections. The F-test is then applied to determine the statistical significance of the observed variances.

Statistical Methods and Analysis

Since an analysis of variance is a method for separating the total variance into its components, the data are classified according to the postulated causes of variation. It is possible to classify the data with respect to each source of variation and the complete classification of these sources is a necessary first step. This can be done with a hierarchic classification. When CHF tests are performed such that data is taken with many test sections of two different designs, it is possible to separate the variance of the data due to the design difference, the variance of the data between test sections and the variance of the data within a test section. For the case where the variance due to 14x14 and 16x16 designs is needed, the hierarchic classification can be shown schematically as in Figure V-1.

In accordance with the hierarchic classification, an analysis of variance table is constructed as shown in Table V-1 (Ref. 17, pg. 165). The true variance between different groups (bundle types) is σ_2^2, the true variance between subgroups (test sections) is σ_1^2 and the true variance within subgroups (test sections) is σ_0^2. These quantities are unknown and must be estimated from the data. M_0 is an estimate of σ_0^2, M_1 is an estimate of $\sigma_0^2 + \bar{n}_1\sigma_1^2$ and M_2 is an estimate of $\sigma_0^2 + \bar{n}_2\sigma_1^2 + \bar{N}\sigma_2^2$. The F test is applied to ratios M_1/M_0 and M_2/M_1.

If a null hypothesis is formulated which states that there is no test section effect or bundle type effect, then the values of σ_1^2 and σ_2^2 are zero. Three independent estimates for σ_0^2 can be obtained;one from the mean square between test bundle types, (M_2), one from the mean square between test sections (M_1), and one from the mean square within test sections (M_0). If we formulate the ratio of M_2/M_1, and of M_1/M_0, the magnitude of these ratios quantifies the extent to which the means square deviate from each other and thus the extent to which the estimates of σ_1^2 and σ_2^2 deviate from zero. Obviously, large deviations

of σ_1^2 and σ_2^2 from zero are a measure of the weakness of the null hypothesis that σ_1^2 and σ_2^2 are zero.

Thus, the F-test is formulated as:

$$F_1 = \frac{M_1}{M_0}$$

$$F_2 = \frac{M_2}{M_1}$$

and a large value of F rejects the null hypothesis at a particular significance level. Tabulated values for significant magnitudes of F for various probabilities and degrees of freedom can be found in many references (see Ref. 17).

A similar procedure is applied to examine the effect of bundle length for the uniform axial power distribution experiments.

The evaluated quantity is the ratio of measured to predicted CHF, therefore, the statistics become a function of the CHF prediction method. In the following analyses, the F test is applied to several sets of data generated in different ways from various types of experiments. It is therefore convenient to subdivide the analysis into cases. These are identified as Cases A thru D. Data points outside the range of the correlation are excluded.

CASE A

This case presents the analysis of variance for uniform axial power distribution data analyzed with TORC/CE-1. The components of variance between bundle groups according to bundle type (14x14 versus 16x16), between test sections and within test sections are estimated. An F-test is applied to the estimates.

CASE B

This case presents the analysis of variance for uniform axial power distribution data analyzed with TORC/CE-1. The components of variance between bundle groups according to bundle length (12.5 ft vs 7.0 ft), between test sections and within test sections are estimated. An F-test is applied to the estimates.

CASE C

This case presents the analysis of variance for non-uniform axial power distribution data analyzed with TORC/CE-1 and the Tong F-factor. The measured to predicted ratio is calculated at the axial position of minimum predicted DNBR. The components of variance between bundle groups according to bundle type (14x14 vs 16x16), between test sections and within test sections are estimated. An F test is applied to the estimates.

CASE D

This case presents the analysis of variance for non-uniform axial power distribution data analyzed with TORC/CE-1 without the Tong F-factor. The measured to predicted ratio is calculated at the axial position of minimum predicted DNBR.

The components of variance between bundle groups according to bundle type (14x14 vs 16x16), between test sections and within test sections are estimated. An F-test is applied to the estimates.

Results

The basic statistics (number of points, mean, standard deviation) for all four cases are given in Table V-2.

The analysis of variance as described above has been applied to the noted cases. When the technique is applied to Case A, results as shown in Table V-3 are obtained. The calculated value of F_1 = 30.34 is much greater than the tabulated value of 2.37 (taken at the .95 confidence level) and F_2 = .0066 is much less than the tabulated value of 7.71 (taken at the .95 confidence level). This shows that the variation from test section to test section is significant but the variation from bundle type to bundle type (14x14 versus 16x16) is not significant. Therefore, the hypothesis that bundle types have no effect cannot be rejected on statistical grounds.

When the technique is applied to Case B results as shown in Table V-4 are obtained. The calculated value of F_1 = 12.71 is much greater than the tabulated value of 2.37 (taken at the 0.95 confidence level) and F_2 = 5.49 is less than the tabulated value of 7.71 (taken at the .95 confidence level). This shows that the variation from test section to test section is significant but the variation from bundle length to bundle length (12.5 ft. versus 7.0 ft.) is not significant. Therefore, the hypothesis that bundle lengths are not different cannot be rejected on statistical grounds. The statistical statement does not necessarily preclude the existence of a length effect. The value of F_2 = 5.49 is relatively close to the tabulated value of 7.71 which may suggest a weak dependence. The length dependence, however, was not included in the CE-1 correlation for the following reasons:

1. Any dependence on heated length is weak.

2. A dependence on heated length is inconsistent with the "local conditions hypothesis" which has been used extensively and successfully for correlating CHF data.

3. The source data include a substantial body of data for the most "adverse condition", i.e., a heated length of 12.5 feet.

4. The true effect of heated length, if any, is likely to be dependent on axial flux shape.

The two cases above are applied to experiments where axial power distribution is uniform. A similar analysis is done for non-uniform axial power distribution data. When the technique is applied to Case C, results as shown in Table V-5 are obtained. The calculated value of F_1 = 45.26 is greater than the tabulated value of 3.07 (taken at the .95 confidence level) and F_2 = .24 is much less than the tabulated value of 18.5 (taken at the .95 confidence level). This shows that the variation from test section to test section is significant but the variation from the bundle type to bundle type (14x14 versus 16x16) is not significant. Therefore the hypothesis that the bundle types have no effect cannot be rejected on statistical grounds.

Similarly results for Case D are shown in Table V-6. The calculated value of F_1 = 100.96 is greater than the tabulated value of 3.07 (taken at the .95 confidence level) and F_2 = .062 is much less than the tabulated value of 18.5 (taken at the .95 confidence level). This shows that the variation from test section to test section is significant but the variation from bundle type to bundle type (14x14 versus 16x16) is not significant. Therefore, the hypothesis that the bundle types have no effect cannot be rejected on statistical grounds.

Conclusions

Several conclusions can be drawn from the results of the analyses performed here. The first and most important is that when using a variety of test and analysis conditions, the hypothesis that the bundle types have no effect cannot be rejected at the .95 confidence level. This is proven by the consistently small values obtained for F_2.

The large values obtained for F_1, show that there is a significant variation between test sections both for uniform and non-uniform data. This behavior is observed quite consistently in C-E's CHF data as well as that from other vendors (Reference 18). An analysis of variance of the Reference 18 data has shown large values of F_1 leading to the conclusion that significant variation between test sections is a random effect inherent in CHF testing. For the uniform data, the between section deviation given in Tables V-3, 4 is very consistent with repeatability analyses in the literature. This is to be expected because of the randomness of the causes for the deviations. The non-uniform data has a greater deviation, however, it is emphasized that the CE-1 correlation was not refit to this data base.

Other aspects of the comparison between the uniform and non-uniform data should be discussed. From Tables V-3, 4, 5, 6, it can be seen that the overall deviation is greater for the non-uniform data than for the uniform data. Furthermore, the overall deviation of the non-uniform data is greater with the Tong F factor than without this factor. As described in Section III the increased deviation within test sections is explained in part by the grid spacing of the C-E design and the favorable effect of spacer grids in non-uniform CHF tests.

In addition, the C-E design diminishes the upstream history effect modelled by the Tong F-factor because of the presence of the grids and the relatively close grid spacing. The F-factor is based on data where no grids are present.

The same discussion applies to the conservative shift of the non-uniform data relative to the uniform data. This conservative shift is evident upon comparison of Figures V-2,3.

It is concluded that the combination of the above noted effects (grids, grid spacing, F-factor) are the causes of the larger deviations and higher means noted in the non-uniform data, and do not cause any concern over the validity of the correlation of the other significant parameters. It is also concluded that the method of application of CE-1 and the F factor proposed for SONGS provides substantial conservatism relative to the C-E DNBR criterion. This criterion states that the minimum DNBR shall be such as to provide at least a 95% probability with 95% confidence that departure from nucleate boiling (DNB) does not occur on a fuel rod having the minimum DNBR during steady-state operation and anticipated transients of moderate frequency. This conservatism is evident in Figures V-2, 3, 4.

TABLE V-1

Sources of Variation	Sum of Squares	Degrees of Freedom	Mean Square	Quantity Estimated by the Mean Square
Between Groups (Bundle Type 14x14 vs 16x16)	S_2	f_2	M_2	$\sigma_o^2+\bar{n}_2\sigma_1^2+\bar{N}\sigma_2^2$
Between Subgroups 'Test Sections)	S_1	f_1	M_1	$\sigma_o^2+\bar{n}_1\sigma_1^2$
Within Subgroups (Test Sections)	S_o	f_o	M_o	σ_o^2

where: σ_o^2 = true variance within subgroups (test sections)

σ_1^2 = true variance between means of subgroups (test sections)

σ_2^2 = true variance between means of groups (bundle types)

$\bar{n}_1, \bar{n}_2$ = estimates of the average number of observations (data points) in subgroup (test sections)

$\bar{N}$ = estimate of the average number of observations (data points) per group (bundle type)

$$M_2 = \frac{S_2}{f_2}$$

$$M_1 = \frac{S_1}{f_1}$$

$$M_o = \frac{S_o}{f_o}$$

TABLE V-2

	Bundle Type	Axial Power Distribution	Bundle Length	No. of Data Points	Mean of Ratio of Measured to Predicted CHF	Std. Dev. of Ratio of Measured to Predicted CHF
Case A,B	14x14	Uniform	7.0 ft	51	1.001	.0493
	14x14	Uniform	7.0	141	1.028	.0580
	14x14	Uniform	12.5	99	.963	.0637
	16x16	Uniform	7.0	114	1.036	.0732
	16x16	Uniform	7.0	169	.991	.0453
	16x16	Uniform	12.5	157	.980	.0764
Case C	14x14	1.68 Top Peaked	12.5	74	1.119	.106
	14x14	1.68 Bottom Peaked	12.5	82	1.287	.130
	16x16	1.46 Symmetric	12.5	108	1.237	.122
	16x16	1.47 Top Peaked	12.5	106	1.254	.083
Case D	14x14	1.68 Top Peaked	12.5	74	1.000	.086
	14x14	1.68 Bottom Peaked	12.5	32	1.170	.091
	16x16	1.46 Symmetric	12.5	108	1.070	.100
	16x16	1.47 Top Peaked	12.5	106	1.155	.066

TABLE V-3

Case A: Uniform Axial Power Distribution Analyzed with TORC/CE-1
Between Bundle Variation Due to Bundle Type Effect

Source of Variation	Sum of Squares	Degrees of Freedom	Mean Square	Estimated Standard Deviation (σ)
Between Bundle Type (14x14 vs 16x16)	.0008	1	.0008	0
Between Test Sections	.4700	4	.1175	.031
Within Test Sections	2.8273	725	.0039	.062

$\overline{n}_1 = 117.4$

$\overline{n}_2 = 126.7$

$\overline{N} = 350.3$

$F_1 = \frac{M_1}{M_o} = 30.34$ (Tabulated value for F for confidence .95 is 2.37)

$F_2 = \frac{M_2}{M_1} = .0066$ (Tabulated value of F for confidence .95 is 7.71

TABLE V-4

Case B: Uniform Axial Power Distribution Analyzed with TORC/CE-1
Between Bundle Variation Due to Length Effect

Source of Variation	Sum of Squares	Degrees of Freedom	Mean Square	Estimated Standard Deviation (σ)
Between Bundle Length (12.5' vs 7.0')	.2725	1	.2725	.025
Between Test Sections	.1983	4	.0496	.020
Within Test Section	2.8273	725	.0039	.062

$\bar{n}_1 = 109.6$

$\bar{n}_2 = 134.7$

$\bar{N} = 332.7$

$F_1 = \frac{M_1}{M_o} = 12.71$ (Tabulated value of F for confidence .95 is 2.37)

$F_2 = \frac{M_2}{M_1} = 5.49$ (Tabulated value of F for confidence .95 is 7.71)

TABLE V-5

Case C: Prediction Method - TORC/CE-1 with Tong F-factor Prediction at Minimum DNBR Location

Source of Variation	Sum of Squares	Degrees of Freedom	Mean Square	Estimated Standard Deviation (σ)
Between Bundle Type (14x14 vs. 16x16)	.1311	1	.1311	0
Between Test Sections	1.1133	2	.5567	.077
Within Test Sections	4.5120	366	.0123	.111

$\overline{n}_1 = 92.4$

$\overline{n}_2 = 90.3$

$\overline{N} = 180.5$

$F_1 = \frac{M_1}{M_o} = 45.26$ (tabulated value of F for confidence .95 is 3.07)

$F_2 = \frac{M_2}{M_1} = .24$ (tabulated value for F for confidence .95 is 18.5)

TABLE V-6

Case D: Prediction Method - TORC/CE-1 Without Tong F-Factor Prediction at Minimum DNBR Location.

Source of Variation	Sum of Squares	Degrees of Freedom	Mean Square	Estimated Standard Deviation (σ)
Between Bundle Type (14x14 vs. 16x16)	.0465	1	.0465	0
Between Test Sections	1.5106	2	.7553	.090
Within Test Sections	2.7380	366	.0075	.087

$\bar{n}_1 = 92.4$

$\bar{n}_2 = 90.3$

$\bar{N} = 180.5$

$F_1 = \frac{M_1}{M_0}$ = 100.96 (Tabulated Value of F for confidence .95 is 3.07)

$F_2 = \frac{M_2}{M_1}$ = .062 (Tabulated value of F for confidence .95 is 18.5)

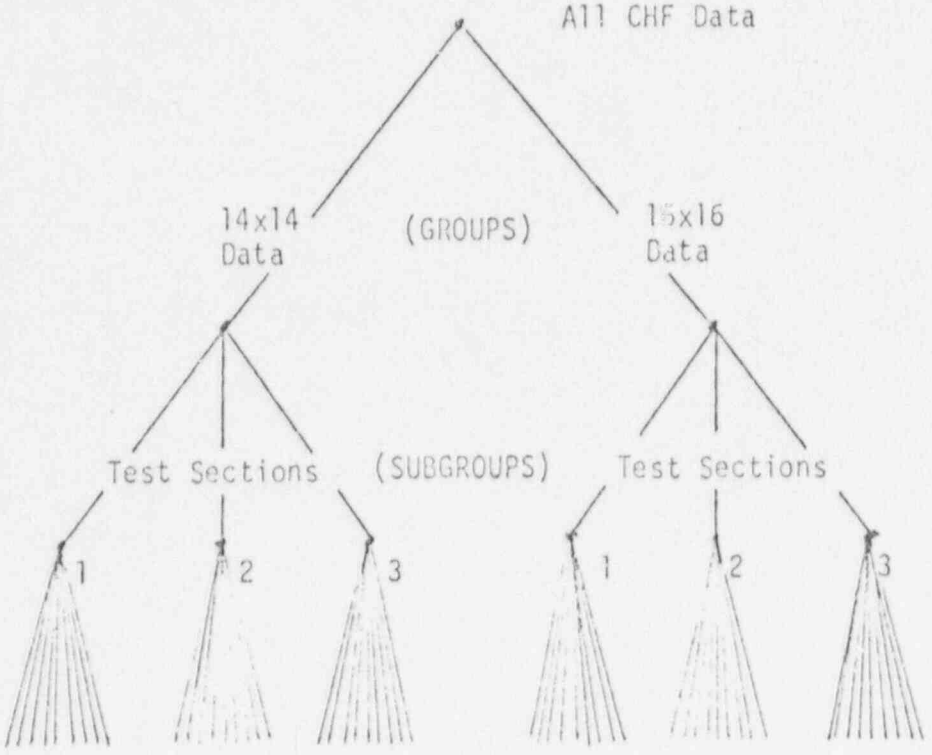

Hierarchic Classification

FIGURE V-1

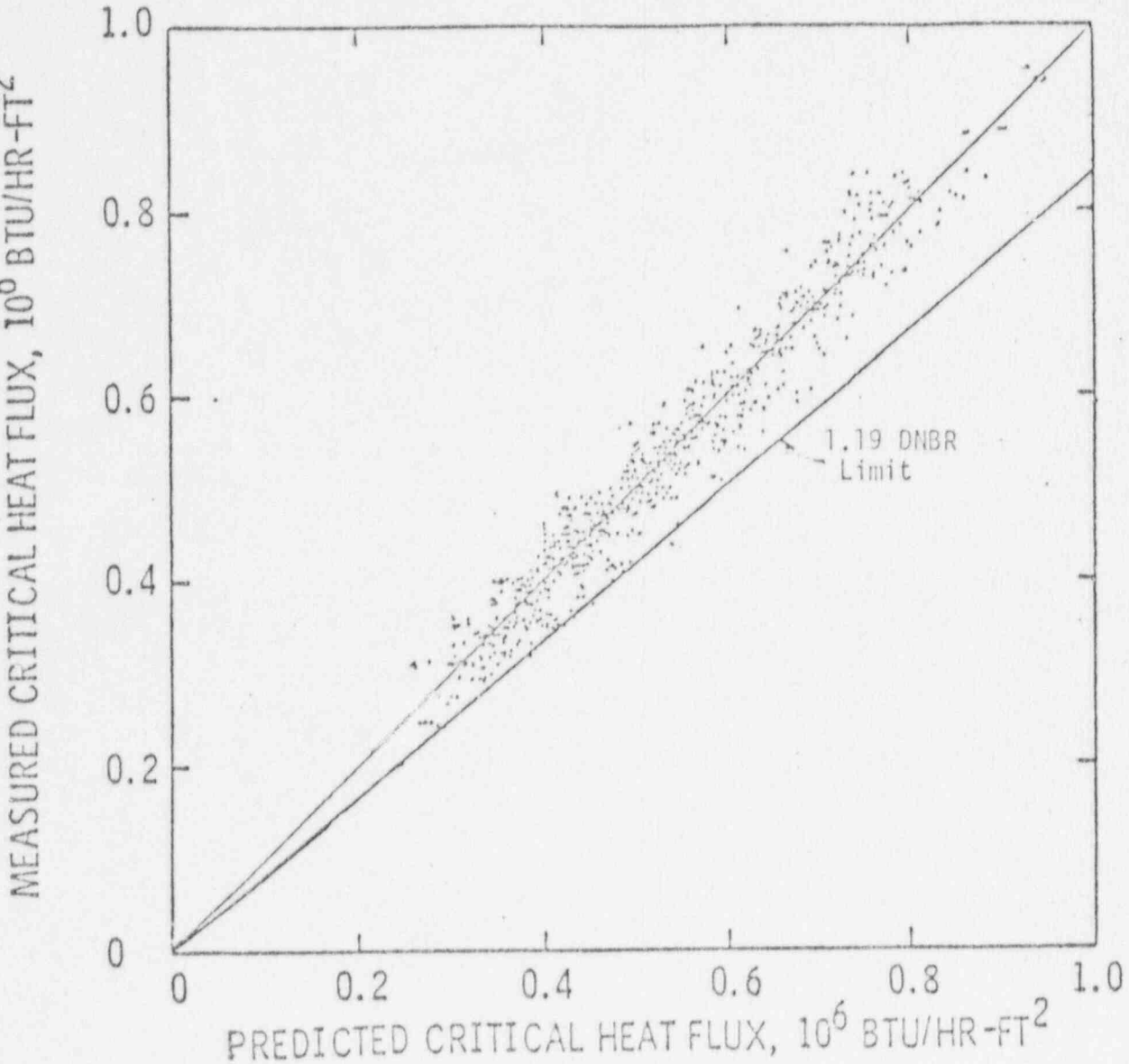

Figure V-2: Measured and Predicted Critical Heat Fluxes from Uniform CHF Tests and the CE-1 Correlation

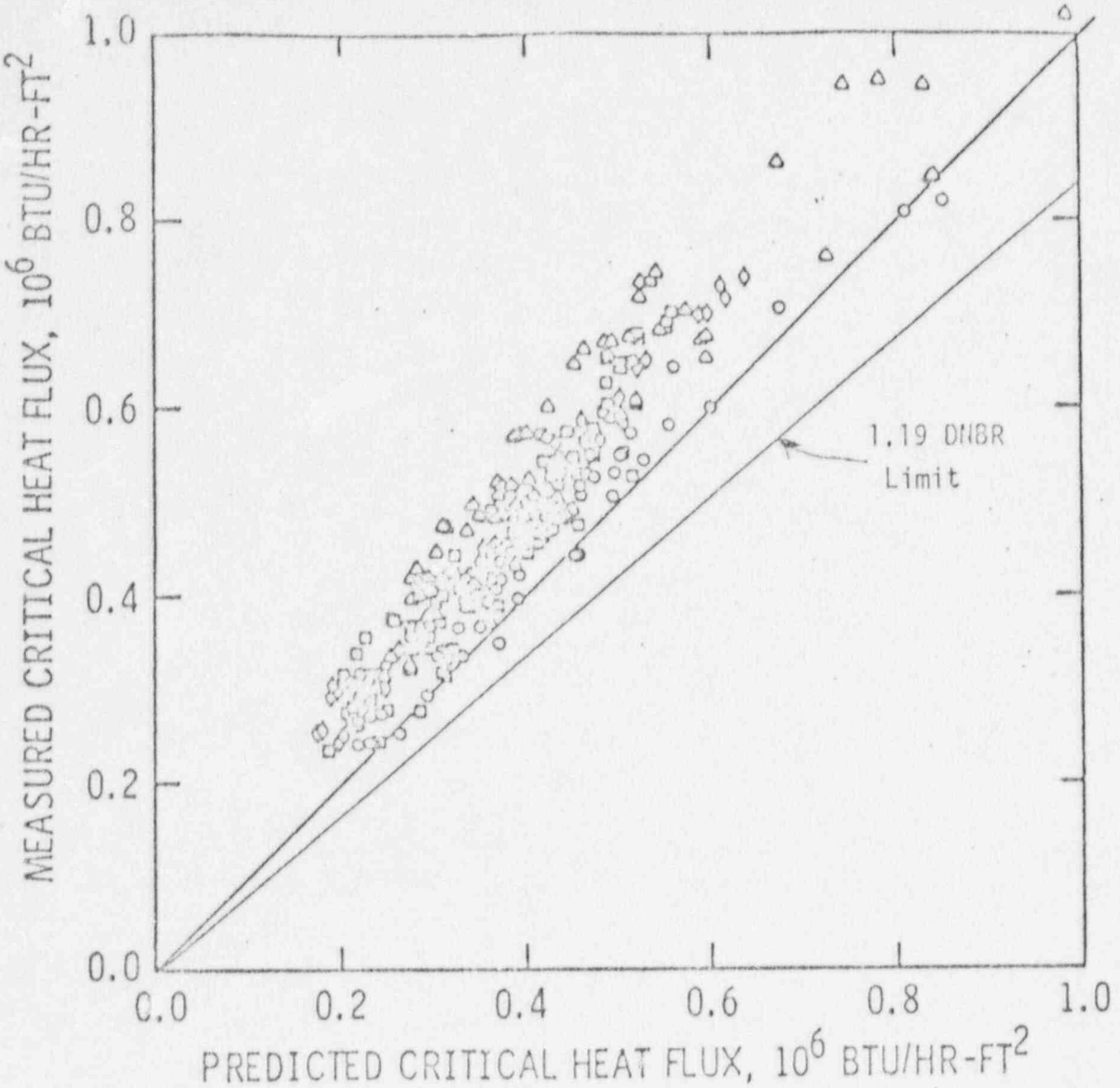

Figure V-3: Measured and Predicted Critical Heat Fluxes from Nonuniform CHF Tests and the CE-1 Correlation

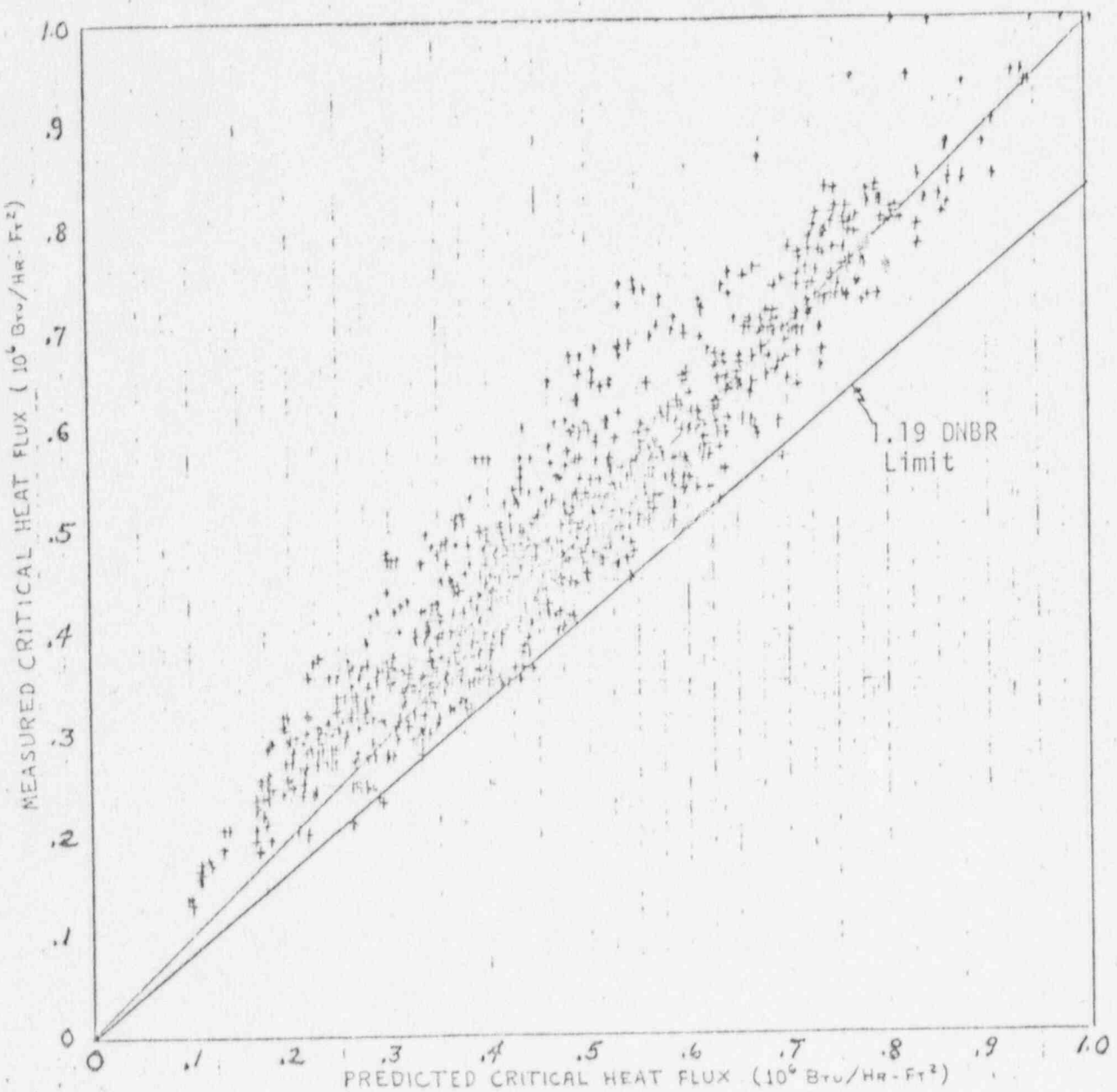

Figure V-4: Measured and Predicted Critical Heat Fluxes for Both Uniform and Nonuniform Test Data with the CE-1 Correlation

VI. REFERENCES

1. L. S. Tong, G. F. Hewitt, "Overall Viewpoint of Flow Boiling CHF Mechanisms", ASME paper 72-HT-54.

2. E. Janssen, "Two-Phase Flow and Heat Transfer in Multirod Geometries", Final Report, GEAP-10347, March 1971.

3. E. Janssen, F. A. Schraub, et al, "Sixteen Rod Heat Flux Investigation, Steam-Water at 600 to 1250 psia", presented at the 1969 Winter Annual ASME Meeting, Los Angeles in session entitled "Two Phase Flow and Heat Transfer in Rod Bundles".

4. B. S. Shiralkar, R. T. Lahey, Jr., "The Effect of Obstacles on a Liquid Film", Trans. ASME, November, 1973, pp. 528-533; ASME paper No. 72-HT-31.

5. R. T. Lahey, Jr., and F. J. Moody, The Thermal Hydraulics of Boiling Water Reactors , ANS, 1977, pp. 97-99.

6. ibid., p. 92.

7. S. A. Chang, R. A. Dean, "Effect of Flow Blockage on Core Power Capability", ASME paper 69-WA/NE-21.

8. L.S. Tong, "A Phenomenological Study of Critical Heat Flux", ASME paper 75-HT-68.

9. G. J. Kidd, Jr., H. W. Hoffman, W. J. Stelzman, "The Temperature Structure and Heat Transfer Characteristics of an Electrically Heated Model of a Seven-Rod Cluster Fuel Element", presented at the 1968 ASME Winter Annual Meeting, New York.

10. S. C. Yao, L. E. Hochreiter, W. J. Leech, "Heat Transfer Augmentation in Rod Bundles Near Spacer Grids", presented at the 1980 ASME Winter Annual Meeting, Chicago.

11. D. C. Groenveld, W. W. Yousef, "Spacing Devices for Nuclear Fuel Bundles: A Survey of Their Effect on CHF, Post-CHF Heat Transfer and Pressure Drop", Proceedings of the ANS/ASME/NRC International Topical Meeting on Nuclear Reactor Thermal Hydraulics, Saratoga Springs, New York, October 5-8, 1980, pp. 1111-1125.

12. "CE-1 Applicability to San Onofre Units 2 & 3 HID-2 Grids", March, 1981, CEN-155(5)-P, response to question 1; dockets 50-361 and 50-362.

13. B. S. Shiralkar, "Two-Phase Flow and Heat Transfer in Multirod Geometries: A Study of the Liquid Film in Adiabatic Air-Water Flow with and without Obstacles", GEAP-10248, October, 1970.

14. L. S. Tong, "Boiling Crisis and Critical Heat Flux", AEC Critical Review Series, August 1972; Library of Congress Catalog Card Number 72-600190.

15. "C-E Critical Heat Flux: Critical Heat Flux Correlation for C-E Fuel Assemblies with Standard Spacer Grids, Part 1, Uniform Axial Power Distribution", CENPD-162-P-A, September, 1976.

16. "C-E Critical Heat Flux: Critical Heat Flux Correlation for C-E Fuel Assemblies with Standard Spacer Grids, Part 2, Nonuniform Axial Power Distributions", CENPD-207-P, June, 1976.

17. "Statistical Methods in Research and Production", O. L. Davies, P. L. Goldsmith, 4th Edition Longmans Group Ltd., London, 1976.

18. "Joint Meeting of the Subcommittee on Reactor Fuels and the Subcommittee on Emergency Core Cooling", Transcript ACRS Meeting, May 5, 1981.

19. "Evaluation of DNB Test Repeatability", K. W. Hill, F. E. Motley, F. F. Cadek, WCAP-8201-A, April 18, 1975.